

# Transient critical regime for light near the three-dimensional Anderson transition

Laura A. Cobus,<sup>1,2,\*</sup> Georg Maret,<sup>3</sup> and Alexandre Aubry<sup>1,†</sup>

<sup>1</sup>*Institut Langevin, ESPCI Paris, CNRS, PSL University, 1 rue Jussieu, F-75005 Paris, France*

<sup>2</sup>*Dodd-Walls Centre for Photonic and Quantum Technologies, New Zealand and Department of Physics, University of Auckland, Private Bag 92109, Auckland, New Zealand*

<sup>3</sup>*Fachbereich Physik, Universität Konstanz, D-78457 Konstanz, Germany*

(Dated: September 24, 2021)

We report on anomalous light transport in the strong scattering regime. Using low-coherence interferometry, we measure the reflection matrix of titanium dioxide powders, revealing crucial features of strong optical scattering which can not be observed with transmission measurements: (i) a subdiffusive regime of transport at early times of flight that is a direct consequence of predominant recurrent scattering loops, and (ii) a transition to a conventional, but extremely slow, diffusive regime at long times. These observations support previous predictions that near-field coupling between scatterers prohibits Anderson localization of light in three-dimensional disordered media.

In disordered media, wave transport can be radically affected by strong scattering. Strong scattering generally occurs when the wavelength of propagating waves is comparable to the scale of structure variations in the medium, so that the waves are extremely sensitive to the size and arrangement of the scatterers. For strong enough disorder and scattering strength, Anderson localization can occur, wherein wave diffusion is suppressed exponentially or even halted altogether [1–5]. In particular, three-dimensional (3D) materials are expected to exhibit a phase transition [6] from conventional diffusion to localization, occurring as disorder/energy is varied, or alternately, as the time spent by the waves exploring the sample increases. This behaviour has been observed experimentally for electrons in doped semiconductors [7, 8], vibrations in elastic networks [4, 9], and cold atoms in random potentials [10–12]. Studies of 3D Anderson localization of light, however, remain inconclusive [13–15]. It is possible that none of the materials tested so far scatter light strongly enough to achieve localization [14, 15]; on the other hand, a number of studies have theorized that the onset of localization is prevented by the dipole-dipole interactions between close-packed scatterers [16–19] which are inherent to the vector nature of light [17, 20]. While supported by preliminary evidence [19], this picture has yet to be conclusively experimentally confirmed.

The experimental search of Anderson localization for light is complicated by absorption and nonlinear effects, which become more important the longer the waves spend inside the sample, and which can imitate signatures of localization [14, 21, 22]. Transmission experiments are particularly affected by fluorescence [14], due to the strong incident beams that are required to overcome noise, absorption, and a low probability of transmission near the localization regime. To avoid these issues, we use low-coherence interferometry. Inspired

by previous studies in acoustics [23, 24] and seismology [25, 26], our approach enables the measurement of time-dependent Green’s functions between points at the surface of a medium which is illuminated by an incoherent light source [27, 28]. This passive type of measurement offers major advantages compared to more conventional methods. First, the reflected wavefield measured via interferometry does not include any signals resulting from spontaneous emission events. Second, a reflection geometry enables the study of: (i) interference phenomena that are precursors of Anderson localization, such as coherent backscattering [29, 30] or recurrent scattering [31, 32], and (ii) the energy ‘halo’ in the early-time limit – a temporal regime which is generally inaccessible in transmission.

In this Letter, low-coherence interferometry is applied to some of the strongest scattering samples which exist for light – titanium dioxide (TiO<sub>2</sub>) powders. We find that the spatio-temporal spreading of the wave energy exhibits two distinct regimes of transport. At short times of flight  $t$ , anomalous diffusion is observed; the spatial extent of the average wave energy,  $w^2(t)$ , scales as  $t^{2/3}$ , and the return probability for the energy density scales as  $t^{-1}$ . These observations are consistent with the scaling theory of localization [33], suggesting the existence of a critical or localized regime. Yet, after a few hundred femtoseconds, a transition towards conventional diffusion is observed;  $w^2(t)$  grows linearly with time, and the temporal decay of the return probability,  $t^{-3/2}$ , is characteristic of the diffusive regime [34]. Diffusion in this regime is very slow, with a diffusion coefficient of  $D \sim 18$  m<sup>2</sup>/s. Interestingly, Naraghi and Dogariu [19] predicted a few years ago that such a transition would be caused by strong near-field coupling between scatterers. While transitory behaviour was observed via measurements of return probability [19], these can be subject to absorption or non-linear effects. Here, we report the first experimental observations of the spatio-temporal energy spread throughout this predicted transition. Our results can be described using the aforementioned model, providing strong evidence for the existence of a transition from a critical (pre-localized) to diffuse regime.

---

\* laura.cobus@auckland.ac.nz

† alexandre.aubry@espci.fr

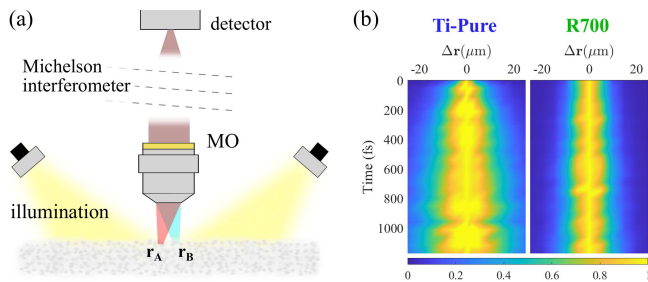


FIG. 1. (a) Low-coherence interferometry measures the cross-correlation between points  $\mathbf{r}_A$  and  $\mathbf{r}_B$  at the sample surface [27] (MO: microscope objective). (b) Normalized intensity profiles  $I(\Delta r, t)/I(0, t)$  are shown for samples Ti-Pure and R700.

Samples investigated in this work were three different types of  $\text{TiO}_2$  powder: a pure anatase phase (Ti-Pure) obtained from Aldrich, and two types of rutile phase powders (R104 and R700) which are commercially available from DuPont as pigments for white paint. Significant Mie scattering resonances can be achieved in these powders, as mean particle size  $\langle d \rangle \sim 400 - 800$  nm [35, 36] is on the order of the wavelength of the illuminating light. The powders were compressed into pastille form to decrease the transport mean free path,  $\ell^*$ , and hence increase optical scattering. Scattering strength can be characterized by  $k_0 \ell^*$ , the product of optical wave number  $k_0$  in vacuum and  $\ell^*$ . A value of  $k_0 \ell^* \sim 1$  indicates very strong scattering, and has been used as an approximate criterion for Anderson localization [33]. Previous measurements have reported  $k_0 \ell^* \sim 5 - 6$ ,  $3 - 4$  and  $2 - 3$  for compressed Ti-Pure, R104 and R700 respectively [37, 38], indicating that light experiences very strong scattering in all three powders. Absorption, on the other hand, is relatively weak, as absorption time  $\tau_a$  is on the order of 1 ns [37].

We measure the spatio-temporal transport of light in these samples using the low-coherence interferometry apparatus introduced by Badon *et al.* [27, 28] (Fig. 1a). A low-coherence broadband light source (650 – 850 nm, radiant flux  $\sim 5 \times 10^5$  W.cm $^{-2}$ ) illuminates the surface of the sample. The backscattered light is collected by a microscope objective and sent to a Michelson interferometer. A CCD camera measures the output of the interferometer, which is the cross-correlation of the scattered wave-fields in each arm of the interferometer. By translating and tilting the mirrors in each arm, a time-dependent reflection matrix  $\mathbf{R}(t)$  can be acquired in a focused basis [28, 39]. This matrix contains the set of impulse responses  $R(\mathbf{r}_A, \mathbf{r}_B, t)$  between points at the surface of the scattering sample,  $\mathbf{r}_A$  and  $\mathbf{r}_B$ . Each of these points acts as a virtual source ( $\mathbf{r}_A$ ) or detector ( $\mathbf{r}_B$ ), whose characteristic size is governed by the resolution length  $\delta r$  of the imaging system, here equal to 1.8  $\mu\text{m}$  [39]. The spatio-temporal behaviour of the wave energy density at the surface of the sample is described by the ensemble average of the impulse response intensity:  $I(\Delta r, t) \equiv \langle |R(\mathbf{r}_A, \mathbf{r}_B, t)|^2 \rangle$ , with  $\Delta r = |\mathbf{r}_A - \mathbf{r}_B|$ . In

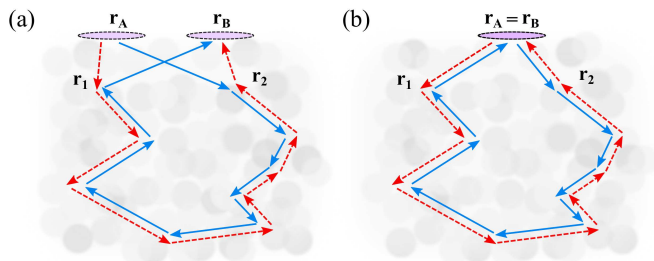


FIG. 2. (a) Coherent backscattering arises from interference between reciprocal paths. Pink ovals represent the size of virtual sources/receivers at  $\mathbf{r}_A$  and  $\mathbf{r}_B$ . (b) When source and receiver coincide, constructive interference is maximized.

practice, this ensemble average is obtained *via* a spatial average over pairs of points  $\mathbf{r}_A$  and  $\mathbf{r}_B$  separated by the same distance  $\Delta r$ . As discussed in the Supplementary Material [39], our passive imaging method enables the extraction of  $I(\Delta r, t)$  from fluorescence and noise contributions that usually pollute active measurements [14, 40].

Figure 1b shows the resulting normalized intensity profile,  $I(\Delta r, t)/I(0, t)$ , for samples Ti-Pure and R700. The difference between samples is immediately obvious: the stronger scattering in R700 limits the spatial spread of energy compared with Ti-Pure. The spread of  $I(\Delta r, t)$  can be quantified by comparing experimental data with theoretical predictions. In the multiple scattering regime,  $I(\Delta r, t)$  can be expressed as the sum of two components. The first is an *incoherent* intensity,  $I_{\text{inc}}$ , which is the incoherent average of the intensity of each individual scattering path. The second is a *coherent* intensity correction  $I_{\text{coh}}$  which takes into account coherent backscattering (CBS) [29, 30], in which waves travelling along pairs of reciprocal paths undergo constructive interference which is not eliminated by the configurational average (Fig. 2).

In real space, the incoherent intensity corresponds to the spatio-temporal spreading of the wave energy density inside the sample – the so-called *diffuse halo*. This spreading can be directly quantified by measuring  $w(t)$ , the *transverse width* of  $I_{\text{inc}}(\Delta r, t)$  [41, 42]. In the diffusive regime,  $I_{\text{inc}}(\Delta r, t)$  can be expressed as follows [34, 39]:

$$I_{\text{inc}}(\Delta r, t) = \frac{ce^{-t/\tau_a}}{2\pi^{3/2}w^3(t)} \exp\left[-\frac{\Delta r^2}{w^2(t)}\right], \quad (1)$$

with

$$w^2(t) = 4D_B t. \quad (2)$$

$D_B$  is the Boltzmann diffusion coefficient [34, 41],  $\tau_a$  is the absorption time, and  $c$  the speed of light in the sample. For anomalous wave transport,  $w^2(t)$  no longer exhibits a linear increase with time, and  $I_{\text{inc}}(\Delta r, t)$  could potentially deviate from a Gaussian shape [4, 43].

The CBS effect ( $I_{\text{coh}}$ ) manifests as an enhancement in the measured MS intensity at  $\Delta r = 0$ . The enhancement factor,  $A$ , can be defined by the relation  $I_{\text{coh}}(0, t) = (A - 1)I_{\text{inc}}(0, t)$ . As  $\Delta r$  increases [Fig.

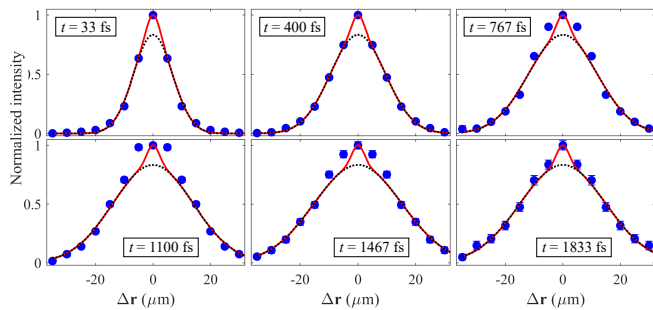


FIG. 3. Normalized intensity profiles  $I(\Delta r, t)/I(0, t)$  for sample R104 (solid symbols) at different times ( $t$ ). Note that experimental error bars are smaller than the symbol size. Red solid lines show theoretical fits with Eq. 3, while black dotted lines represent only the diffuse halo term of Eq. 3.

2(b)], the enhancement falls off, giving rise to a peak  $F(\Delta r)$  of characteristic width  $\delta r$  [39]. While in  $\mathbf{k}$ -space this CBS peak narrows as time increases [44–46], in real-space its shape is stationary [42, 47, 48]. Ideally, for an experiment with point-like sources and detectors on the medium surface, this CBS peak has the form  $I_{\text{coh}}(\Delta r, t) \propto [\sin(k\Delta r)/k\Delta r]^2 \exp(-r/\ell_s)$  ( $\ell_s$  is the scattering mean free path) with an enhancement of  $A = 2$  [47]. Here, the diffraction limit of our imaging system changes the CBS peak shape to an Airy disk. Lower-order aberrations (non-ideal focus and/or astigmatism) can furthermore cause both an increase in CBS peak width and decrease in relative amplitude ( $A < 2$ ) [39].

Altogether,  $I(\Delta r, t)$  in the diffusion approximation has the form of a narrow CBS peak on top of a broader time-dependent diffusive halo. The normalized intensity profile can then be written as [39]

$$\frac{I(\Delta r, t)}{I(0, t)} = \frac{1}{A} e^{-\Delta r^2/w^2(t)} + \left(1 - \frac{1}{A}\right) F(\Delta r). \quad (3)$$

Figure 3 shows  $I(\Delta r, t)/I(0, t)$  for sample R104 for six times-of-flight  $t$  spanning the entire measurement range. The spatio-temporal spreading of wave energy is clearly exhibited, as is a small and constant CBS enhancement around  $\Delta r = 0$ . To quantify the energy spread in each sample, the experimental  $I(\Delta r, t)$  was compared with the prediction of Eq. 3. Fit parameters were  $w^2(t)$  (a free parameter for each time  $t$ ), and  $A$ , which was held constant over time. Note that while the shape of  $I(\Delta r, t)$  is only strictly expected to be Gaussian when the diffusion approximation applies,  $w^2(t)$  can still give a good quantification of spatio-temporal energy spreading [5], and that in any case,  $I(\Delta r, t)$  is well-described by a Gaussian for the entire time range under investigation (Fig. 3). The fitting gives very small values for  $A$  which are caused by aberration effects in the experimental setup [39]:  $A = 1.12$  for Ti-Pure,  $A = 1.2$  for R104, and  $A = 1.1$  for R700. Results for  $w^2(t)$ , however, do not agree with the diffusive prediction of Eq. 2. This implies that our theoretical model must be altered to take into

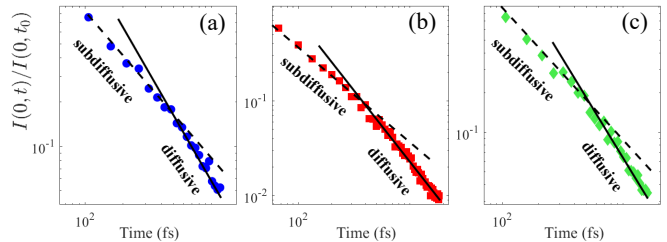


FIG. 4. Return probability  $I(0, t)$  normalized by its value at time  $t_0 = 53$  fs for (a) Ti-Pure, (b) R104 and (c) R700 (symbols). Lines following  $t^{-3/2}$  (solid, diffusive) and  $t^{-1}$  (dashed, subdiffusive) are guides to the eye, not fits.

account the extreme strong scattering of our samples.

Compared with conventional diffusion, a key feature of the strong scattering regime ( $k\ell^* \sim 1$ ) is the predominance of recurrent scattering ‘loops’, *i.e.* an increased probability for waves to pass nearby areas that they have previously visited [32, 49, 50]. The time-dependence of this *return probability* can be directly quantified in the reflection geometry by observing the back-scattered intensity at the source location,  $I(0, t)$  [Fig. 2(b)]. Figure 4 shows  $I(0, t)$  for all three samples. As absorption is negligible for the time range of our measurements,  $I(0, t)$  should scale as  $t^{-3/2}$  in the diffusive regime (Eq. 1). As the system approaches a transition between diffusion and Anderson localization, the slowing of diffusion can be modeled as a scale-dependent diffusion process [51]. Based on the scaling theory of localization [33], the diffusion coefficient should scale with time as [1, 2, 51]

$$D(t) \simeq \frac{(D_0 \ell^*)^{2/3}}{(6t)^{1/3}}, \quad (4)$$

with  $D_0$  the diffusion constant in the absence of rescaling. Replacing  $D_B$  by the renormalized diffusion coefficient  $D(t)$  in Eq. 1 gives the following scaling for the return probability in the localized regime:  $I(0, t) \propto t^{-1}$  [52].

Comparison of these theoretical predictions with the experimental data reveals the existence of a transition between two transport regimes at a critical time  $\tau_c \sim 425$  fs for Ti-Pure,  $\tau_c \sim 400$  fs for R104 and  $\tau_c \sim 480$  fs for R700 (Fig. 4). Before  $\tau_c$ , the return probability scales as  $t^{-1}$  which is characteristic of a regime of continuously renormalized diffusion (which falls into the more general category of *subdiffusion*). After the transition ( $t > \tau_c$ ), the return probability scales as  $t^{-3/2}$  as expected for diffusion. Naraghi and Dogariu [19] have predicted such a transition, proposing that near-field coupling between scatterers constitutes a ‘leak’ of energy from propagating paths (e.g. Fig. 2) to evanescent channels. This effect lessens the constructive interference created by recurrent scattering paths, preventing the localization of wave resonances. By modeling recurrent scattering and near-field coupling as competing mechanisms, the critical time can be theoretically expressed as  $\tau_c \sim \lambda^2/(3c\ell^*\rho)$  [19, 39], where  $\rho$  is the ratio between the near-field and transport cross-sections. Using the values of  $\ell^* \sim 0.3 \mu\text{m}$  [38]

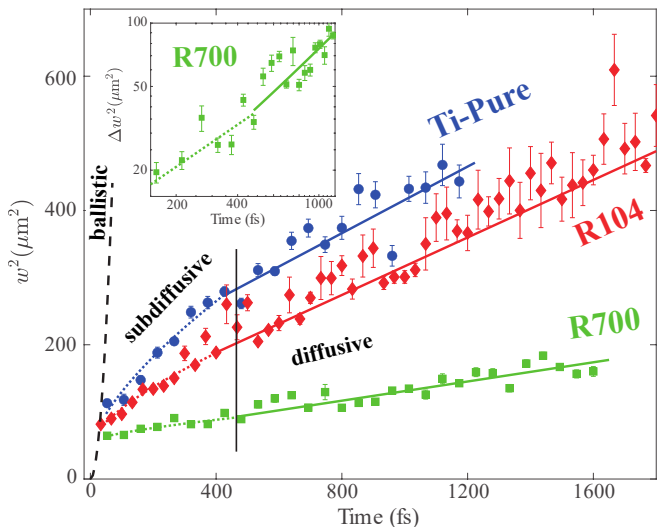


FIG. 5. Transverse width  $w^2(t)$  for all three samples (symbols). Error bars represent the uncertainty in  $w^2(t)$  due to the (weighted) fitting of  $I(\Delta r, t)/I(0, t)$  with Eq. 3. Linear fits to the data (solid lines) give  $D$ , for each sample. In the regime of renormalized diffusion ( $t < \tau_c$ ), the data is fit with Eq. 5 (dotted lines). The ballistic light line (dashed black line), indicates the lower limit for  $w^2(t)$ . Inset:  $\Delta w^2$  through the subdiffusion-diffusion transition for R700 (log-log scale).

and refractive index  $n \sim 2.7$  [37], measured in R700 at  $\lambda_0 = 700$  nm, and taking  $\tau_c \sim 480$  fs (Fig. 4c), we find  $\rho \sim 10^{-2}$ . While this small value seems to imply that the energy leak into evanescent channels is negligible, it is for only a few scattering events; in the long-time limit the sheer number of these events results in the extinction of localization and the recovery of diffusion. We note that the observed values of  $\tau_c$  do not scale with  $\ell^*$ . This is likely due to variation in  $\rho$ ; although each sample was compressed with the same force, differences in particle size/shape could cause the volume fraction to vary slightly between samples. The differing chemical composition of the samples could also affect the near-field scattering cross-section.

The transition from subdiffusion to diffusion is exhibited more directly in the spatio-temporal spread of wave energy, here quantified via  $w(t)$ . As shown in Figure 5,  $w^2(t)$  increases linearly with time at long times of flight ( $t > \tau_c$ ). This behaviour is predicted by the diffusion approximation, in which  $w^2(t) = 4Dt + w_c^2$ , where  $w_c^2$  is the lateral extension of the energy halo at critical time  $\tau_c$ . Linear fits to  $w^2(t)$  give a direct measurement of  $D$  for each sample:  $D = 62 \pm 10$  m<sup>2</sup>/s for Ti-Pure,  $D = 54 \pm 6$  m<sup>2</sup>/s for R104, and  $D = 18 \pm 9$  m<sup>2</sup>/s for R700. The measured value of  $D$  for R700 is in excellent agreement with previous wavelength-dependent measurements performed in transmission [37]:  $D \approx 18$  m<sup>2</sup>/s for  $\lambda = 700$  nm [38]. Other previously reported values are  $D \sim 20$  m<sup>2</sup>/s for Ti-Pure and  $D \sim 18 - 38$  m<sup>2</sup>/s for R104 [37], which differ from ours, but were performed for wavelengths at the lowest range of our experimental

spectrum. Moreover, the relative values of  $D$  that we obtain are logical in light of the differing values of  $k\ell^*$  reported for the three samples [37, 38].

For  $t < \tau_c$ , the time dependence of the return probability (Fig. 4) indicates the renormalization of diffusion. For these times, the behavior of  $w^2(t)$  can be predicted by substituting  $D(t)$  (Eq. 4) for  $D_B$  in Eq. 2, giving

$$w^2(t) = \frac{4}{\sqrt[3]{6}}(D_0\ell^*t)^{2/3} + w_0^2, \quad (5)$$

where  $w_0^2$  is the size of the diffuse halo extrapolated to time  $t = 0$ . Fitting the experimental  $w^2(t)$  curves with Eq. 5 confirms the scaling of  $w^2(t)$  as  $t^{2/3}$  for  $t < \tau_c$ . The subdiffusion-diffusion transition can be more clearly seen by plotting  $\Delta w^2 = w^2 - w_0^2$  on a log-log scale – this is shown for R700 in the inset of Fig. 5. Using the value of  $\ell^*$  measured for this sample at  $\lambda = 700$  nm [38], an estimate of  $D_0$  can be extracted from the fitting process described by Eq. 5. Remarkably, we find a value of  $D_0 \sim 15$  m<sup>2</sup>/s, which agrees within error with  $D \sim 18 \pm 9$  m<sup>2</sup>/s measured from a linear fit of  $w^2(t)$  in the diffuse regime (Eq. 2).

A remaining question concerns the transport of light at very early times. The earliest measured point of  $w^2(t)$ , at  $t \sim 50$  fs, is close to the ballistic light line  $w(t) = c_0t$  (Fig. 5). Only super-diffusive – if not ballistic – transport could account for such rapid growth of the diffuse halo. One possible explanation is the existence of ballistic waves propagating at the surface of the scattering sample; at early times, this contribution would dominate the observed dynamics of the diffuse halo.

In conclusion, we have quantified the spatio-temporal optical energy transport in a strongly scattering regime across a wide range of time scales. Strikingly, we observe a transition between a regime of continuously renormalized diffusion at early times, and a conventional diffusion regime at long times. The observed transition is a manifestation of near-field couplings between scatterers that are inherent to the vector nature of light, and which dominate over recurrent scattering at long times. This effect may explain the elusive 3D Anderson localization of electromagnetic waves. In the long-time diffusive regime, the extremely slow values for the diffusion coefficient  $D$  are in agreement with previous experimental measurements performed in transmission [38]. The application of our experimental method to such challenging samples also illuminates the advantages of passive measurements to probe wave phenomena in a strong scattering regime, where non-linear effects, fluorescence, and noise can be increasingly dominant over signals of interest [14, 40]. In the future, a passive measurement of the reflection matrix will constitute a relevant tool to study not only the statistics of the mean intensity, but also the field-field correlations under the framework of random matrix theory [53, 54].

## ACKNOWLEDGMENTS

The authors would like to thank Nicolas Lequeux for his help in fabricating the samples, Lukas Schertel for his advice and support, and Sergey Skipetrov and Bart van Tiggelen for fruitful discussions. This project has received funding from the Labex WIFI (Laboratory of Excellence within the French Program Investments for the Future, ANR-10-LABX-24 and ANR-10-IDEX-0001-02

PSL\*) and the Agence Nationale de la Recherche (ANR-14-CE26-0032, Research Project LOVE). L. A. C. acknowledges financial support from the European Union's Horizon 2020 research and innovation programme under the Marie Skłodowska-Curie grant agreement No. 744840. A. A. acknowledges financial support from the European Research Council (ERC) under the European Union's Horizon 2020 research and innovation programme (grant agreement No. 819261).

- 
- [1] P. W. Anderson, Absence of Diffusion in Certain Random Lattices, *Phys. Rev.* **109**, 1492 (1958).
- [2] S. John, Electromagnetic Absorption in a Disordered Medium near a Photon Mobility Edge, *Phys. Rev. Lett.* **53**, 2169 (1984).
- [3] S. John, Localization of Light, *Phys. Today* **44**, 32 (1991).
- [4] H. Hu, A. Strybulevych, J. H. Page, S. E. Skipetrov, and B. A. van Tiggelen, Localization of ultrasound in a three-dimensional elastic network, *Nat. Phys.* **4**, 945 (2008).
- [5] L. A. Cobus, W. K. Hildebrand, S. E. Skipetrov, B. A. van Tiggelen, and J. H. Page, Transverse confinement of ultrasound through the Anderson transition in three-dimensional mesoglasses, *Phys. Rev. B* **98**, 214201 (2018).
- [6] F. Evers and A. D. Mirlin, Anderson transitions, *Rev. Mod. Phys.* **80**, 1355 (2008).
- [7] T. Rosenbaum, K. Andres, G. Thomas, and R. Bhatt, Sharp metal-insulator transition in a random solid, *Phys. Rev. Lett.* **45** (1980).
- [8] P. A. Lee and T. V. Ramakrishnan, Disordered electronic systems, *Rev. Mod. Phys.* **57**, 287 (1985).
- [9] L. A. Cobus, A. Aubry, S. E. Skipetrov, B. A. van Tiggelen, A. Derode, and J. H. Page, Anderson mobility gap probed by dynamic coherent backscattering, *Phys. Rev. Lett.* **116**, 193901 (2016).
- [10] J. Chabé, G. Lemarié, B. Grémaud, D. Delande, P. Szriftgiser, and J. Garreau, Experimental experimental observation of the Anderson metal-insulator transition with atomic matter waves, *Phys. Rev. Lett.* **101**, 255702 (2008).
- [11] S. S. Kondov, W. R. McGehee, J. J. Zirbel, and B. DeMarco, Three-dimensional Anderson localization of ultracold matter, *Science* **334**, 66 (2011).
- [12] F. Jendrzejewski, A. Bernard, K. Müller, P. Cheinet, V. Josse, M. Piraud, L. Pezzé, L. Sanchez-Palencia, A. Aspect, and P. Bouyer, Three-dimensional localization of ultracold atoms in an optical disordered potential, *Nat. Phys.* **8**, 398 (2012).
- [13] T. van der Beek, P. Barthelemy, P. M. Johnson, D. S. Wiersma, and A. Lagendijk, Light transport through disordered layers of dense gallium arsenide submicron particles, *Phys. Rev. B* **85**, 1 (2012).
- [14] T. Sperling, L. Schertel, M. Ackermann, G. J. Aubry, C. M. Aegerter, and G. Maret, Can 3D light localization be reached in 'white paint'?, *New J. Phys.* **18**, 13039 (2016).
- [15] S. E. Skipetrov and J. H. Page, Red light for Anderson localization, *New J. Phys.* **18**, 21001 (2016).
- [16] S. John, *Phys. Today* **45**, 122 (1992).
- [17] S. E. Skipetrov and I. M. Sokolov, Absence of anderson localization of light in a random ensemble of point scatterers, *Phys. Rev. Lett.* **112**, 1 (2014).
- [18] L. Bellando, A. Gero, E. Akkermans, and R. Kaiser, Cooperative effects and disorder: A scaling analysis of the spectrum of the effective atomic Hamiltonian, *Phys. Rev. A* **90**, 1 (2014).
- [19] R. R. Naraghi and A. Dogariu, Phase transitions in diffusion of light, *Phys. Rev. Lett.* **117**, 1 (2016).
- [20] N. Cherroret, D. Delande, and B. A. Van Tiggelen, Induced dipole-dipole interactions in light diffusion from point dipoles, *Phys. Rev. A* **94**, 1 (2016).
- [21] D. S. Wiersma, P. Bartolini, A. Lagendijk, and R. Righini, Localization of light in a disordered medium, *Nature* **390**, 671 (1997).
- [22] F. Scheffold, R. Lenke, R. Tweert, and G. Maret, Localization or classical diffusion of light?, *Nature* **398**, 206 (1999).
- [23] R. L. Weaver and O. I. Lobkis, Ultrasonics without a source: thermal fluctuation correlations at MHz frequencies, *Phys. Rev. Lett.* **87**, 134301 (2001).
- [24] A. Derode, E. Larose, M. Campillo, and M. Fink, How to estimate the Green's function of a heterogeneous medium between two passive sensors? Application to acoustic waves, *Appl. Phys. Lett.* **83**, 3054 (2003).
- [25] M. Campillo and A. Paul, Long-Range Correlations in the Diffuse Seismic Coda, *Science* **299**, 547 (2003).
- [26] E. Larose, L. Margerin, A. Derode, B. A. van Tiggelen, M. Campillo, N. Shapiro, A. Paul, L. Stehly, and M. Tanter, "Correlation of random wave-fields: an interdisciplinary review, *Geophysics* **71**, SI11 (2006).
- [27] A. Badon, G. Lerosey, C. Boccara, M. Fink, and A. Aubry, Retrieving Time-Dependent Green's Functions in Optics with Low-Coherence Interferometry, *Phys. Rev. Lett.* **114**, 023901 (2015).
- [28] A. Badon, D. Li, G. Lerosey, A. C. Boccara, M. Fink, and A. Aubry, Spatio-Temporal Imaging of Light Transport in Highly Scattering Media under White Light Illumination, *Optica* **3**, 11 (2016).
- [29] P.-E. Wolf and G. Maret, Weak localization and coherent backscattering of photons in disordered media, *Phys. Rev. Lett.* **55**, 2696 (1985).
- [30] M. P. V. Albada and A. Lagendijk, Observation of weak localization of light in a random medium, *Phys. Rev. Lett.* **55**, 2692 (1985).
- [31] D. S. Wiersma, M. P. van Albada, B. A. van Tiggelen, and A. Lagendijk, Experimental Evidence for Recurrent Multiple Scattering Events of Light in Disordered Media, *Phys. Rev. Lett.* **74**, 4193 (1995).

- [32] A. Aubry, L. A. Cobus, S. E. Skipetrov, B. A. van Tiggelen, A. Derode, and J. H. Page, Recurrent scattering and memory effect at the anderson localization transition, *Phys. Rev. Lett.* **112**, 043903 (2014).
- [33] E. Abrahams, P. W. Anderson, D. C. Licciardello, and T. V. Ramakrishnan, Scaling theory of localization: Absence of quantum diffusion in two dimensions, *Phys. Rev. Lett.* **42**, 673 (1979).
- [34] M. S. Patterson, B. Chance, and B. C. Wilson, Time resolved reflectance and transmittance for the noninvasive measurement of tissue optical properties, *Appl. Opt.* **28**, 2331 (1989).
- [35] M. Störzer, *Anderson Localization of Light*, Ph.D. thesis, Universität Konstanz (2006).
- [36] W. Bühner, *Anderson Localization of Light in the Presence of Non-linear Effects*, Ph.D. thesis, Universität Konstanz (2012).
- [37] T. Sperling, *The experimental search for Anderson localization of light in three-dimensions*, Ph.D. thesis, Universität Konstanz (2015).
- [38] L. Schertel, I. Wimmer, B. P., C. M. Aegerter, G. Maret, S. Polarz, and G. J. Aubry, Tunable high-index photonic glasses, *Phys. Rev. M* **3**, 015203 (2019).
- [39] See Supplemental Material at ... for further details.
- [40] T. Sperling, W. Bühner, C. M. Aegerter, and G. Maret, Direct determination of the transition to localization of light in three dimensions, *Nat. Photonics* **7**, 48 (2013).
- [41] J. H. Page, H. P. Schriemer, A. E. Bailey, and D. A. Weitz, Experimental test of the diffusion approximation for multiply scattered sound, *Phys. Rev. E* **52**, 3106 (1995).
- [42] A. Aubry and A. Derode, Ultrasonic imaging of highly scattering media from local measurements of the diffusion constant: Separation of coherent and incoherent intensities, *Phys. Rev. E* **75**, 026602 (2007).
- [43] N. Cherroret, S. E. Skipetrov, and B. A. van Tiggelen, Transverse confinement of waves in three-dimensional random media, *Phys. Rev. E* **82** (2010).
- [44] R. Vreeker, M. P. van Albada, R. Sprik, and A. Lagendijk, Femtosecond time-resolved measurements of weak localization of light, *Phys. Lett. A* **132**, 51 (1988).
- [45] A. Tourin, A. Derode, P. Roux, B. A. van Tiggelen, and M. Fink, Time-dependent coherent backscattering of acoustic waves, *Physical Review Letters* **79**, 3637 (1997).
- [46] A. Aubry, A. Derode, P. Roux, and A. Tourin, Coherent backscattering and far-field beamforming in acoustics, *The Journal of the Acoustical Society of America* **121**, 70 (2007).
- [47] L. Margerin, M. Campillo, and B. A. van Tiggelen, Coherent backscattering of acoustic waves in the near field, *Geophys. J. Int.* **145**, 593 (2001).
- [48] B. A. van Tiggelen, L. Margerin, and M. Campillo, Coherent backscattering of elastic waves: Specific role of source, polarization, and near field, *J. Acoust. Soc. Am.* **110**, 1291 (2001).
- [49] D. Vollhardt and P. Wölfle, Scaling equations from a self-consistent theory of Anderson localization, *Phys. Rev. Lett.* **48**, 699 (1982).
- [50] S. E. Skipetrov and B. A. van Tiggelen, Dynamics of Anderson localization in open 3D media, *Phys. Rev. Lett.* **96**, 043902 (2006), 0508726v2.
- [51] K. M. Douglass, S. John, T. Suezaki, G. A. Ozin, and A. Dogariu, Anomalous flow of light near a photonic crystal pseudo-gap, *Opt. Express* **19**, 25320 (2011).
- [52] The temporal scaling laws of the return probability differ from the ones considered in a previous acoustics work [32]. While the previous study considered the far-field reflectance of the medium, *i.e.* an energy flux density [34], here we probe the energy density at the sample surface.
- [53] C. W. J. Beenakker, Random-matrix theory of quantum transport, *Rev. Mod. Phys.* **69**, 731 (1997).
- [54] B. Gérardin, J. Laurent, A. Derode, C. Prada, and A. Aubry, Full transmission and reflection of waves propagating through a maze of disorder, *Phys. Rev. Lett.* **113**, 173901 (2014).